# Site-specific and doping-dependent electronic structure of $YBa_2Cu_3O_x$ probed by O 1s and Cu 2p x-ray-absorption spectroscopy

N. Nücker, E. Pellegrin, and P. Schweiss
*Forschungszentrum Karlsruhe, Institut für Nukleare Festkörperphysik, Postfach 3640, D-76021 Karlsruhe, Germany*

J. Fink
*Institut für Festkörper- und Werkstofforschung, Postfach, 01171 Dresden, Federal Republic of Germany*

S. L. Molodtsov, C. T. Simmons, and G. Kaindl
*Institut für Experimentalphysik, Freie Universität Berlin, Arnimallee 14, 14195 Berlin, Federal Republic of Germany*

W. Frentrup
*Institut für Ionen- und Elektronenphysik, Humboldt-Universität zu Berlin, Invalidenstraße 110, 10115 Berlin, Federal Republic of Germany*

A. Erb and G. Müller-Vogt
*Kristall- und Materiallabor, Universität Karlsruhe, 76133 Karlsruhe, Federal Republic of Germany*
(Received 26 August 1994; revised manuscript received 21 November 1994)

The electronic structure of the $CuO_2$ planes and $CuO_3$ chains in single-domain crystals of $YBa_2Cu_3O_x$ has been investigated as a function of oxygen concentration ($6 \leq x \leq 7$) using polarization-dependent x-ray-absorption spectroscopy of the O 1s and Cu 2p core levels. The polarization-dependent observation of unoccupied states with O and with Cu orbital character parallel to the *a*, *b*, and *c* axes of the crystals allows the determination of the number of hole states in Cu $3d_{x^2-y^2}$ and O $2p_{x,y}$ orbitals in the $CuO_2$ planes as well as in Cu $3d_{y^2-z^2}$ and O $2p_{y,z}$ orbitals in the $CuO_3$ chains. States with Cu $3d_{3z^2-r^2}$ orbital character contribute less than 10% to the total number of states near the Fermi level. The number of holes in the planes and in the chains is found to be correlated with the superconducting transition temperature.

## I. INTRODUCTION

High-temperature superconductors (HTSC's) may be described by $CuO_2$ layers embedded in block layers which are presumably responsible for superconductivity. These block layers are necessary for the stabilization of the $CuO_2$ layers and they determine the occurrence of physical properties such as, for example, magnetic order, conductivity, and superconductivity in the $CuO_2$ layers. Moreover, these properties can be tuned by modifications of the block layers, leading to changes of internal pressure or doping concentration in the $CuO_2$ planes.

Since the discovery of the first HTSC,[1] an enormous number of theoretical and experimental investigations has been performed and a wealth of knowledge on this class of materials has been obtained. However, the main question concerning the origin of superconductivity has not yet been answered. An important ingredient for the understanding of superconductivity is the knowledge of the electronic structure of these materials. The early theoretical investigations of the electronic states by band-structure calculations in the local-density approximation (LDA) failed to predict the band gap and the antiferromagnetic order in $La_2CuO_4$,[2] because of the strong on-site correlations on the copper sites. However, this situation has improved recently due to the introduction of self-interaction corrections[3–5] (SIC) to the local-spin-density (LSD) formalism.

In this paper the investigation of unoccupied electronic states in $YBa_2Cu_3O_x$ having Cu and O character is described as a function of oxygen stoichiometry. In the following, and as shown in Fig. 1, we will adopt the notation of Cu(1) and Cu(2), respectively, for the copper sites in the chain and the two planes per formula unit, and of O(1), O(2), O(3), and O(4) for, respectively, the oxygen sites between the Cu(1) atoms on the *b* axis, those of the plane on the *a* and *b* axes, and the apical site. In the undoped case, $YBa_2Cu_3O_6$ is in a tetragonal phase due to the absence of the O(1) atoms. With increasing oxygen content, a transition to the orthorhombic phase occurs near $x = 6.3$,[6] due to the formation of chain fragments. Upon further doping, a tendency for ordering of oxygen atoms in chains or chain fragments has been observed.[7–11] In $YBa_2Cu_3O_7$, complete $CuO_3$-chains extend along the crystallographic *b* direction.

Tetragonal $YBa_2Cu_3O_6$ is an insulator. Near the transition to the orthorhombic phase, $YBa_2Cu_3O_x$ becomes metallic and superconducting. For higher oxygen contents the superconducting transition temperature $T_c$ is observed to rise stepwise (with a plateau near $x = 6.6$ and $T_c \approx 60$ K (Ref. 12) to a maximum value of 91 K for $x$ near 6.93.[13] In the intermediate region, $T_c$ depends on

 

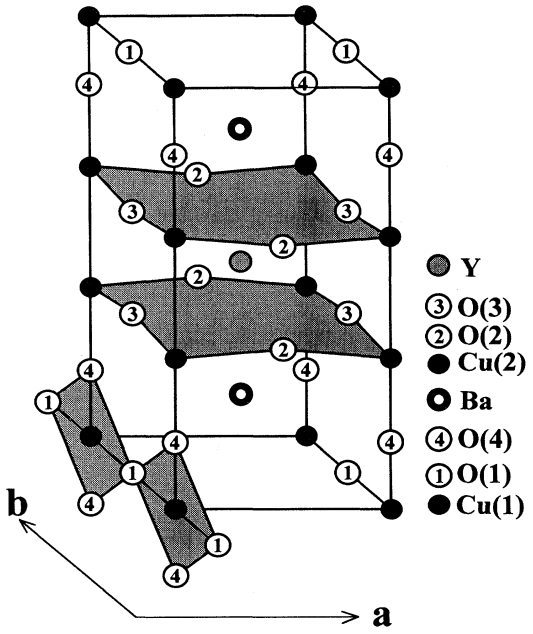


FIG. 1. Unit cell of $YBa_2Cu_3O_7$. The $CuO_2$ planes and the $CuO_3$ chains are indicated by a grey tone.

the order within the chains.[14,15]

In an ionic picture, $YBa_2Cu_3O_6$ can be understood as composed of trivalent Y, divalent Ba, and divalent O. The Cu(1) atoms in $YBa_2Cu_3O_6$ are twofold coordinated with O(4) atoms and hence are in the monovalent state. The two Cu(2) atoms per formula unit of the planes will have a valency of $2^+$. Upon introducing oxygen up to $x=6.5$, we may argue that extra holes will form $Cu(1)^{++}$. The latter might be expected since with the change of the copper coordination from twofold to fourfold, a change from formally monovalent ($Cu^+$) to divalent copper ($Cu^{++}$) is commonly observed. The occurrence of $Cu(1)^+$ for low oxygen contents in $YBa_2Cu_3O_x$ was derived from the line shape and the main line to satellite ratio as observed in Cu $2p$ x-ray photoemission spectra (XPS).[16,17] Polarized Cu $1s$ x-ray-absorption spectroscopy[18,19] (XAS) reveals an excitation into Cu $4p$ orbitals in the $a,b$ plane, which is taken as evidence for $Cu^+$. Further evidence for $Cu^+$ came from nuclear magnetic resonance[20] (NMR) and nuclear quadrupolar resonance (NQR).[21] Optical reflectivity[22] and electron-energy-loss spectroscopy[23] (EELS) investigations show a sharp feature at about 4 eV probably caused by an $O(4)\text{-}Cu(1)^+\text{-}O(4)$ dumbbell. At oxygen contents above $x=6.5$ it was expected that the extra holes are doped to Cu(2) transforming it partly to $Cu^{3+}$. This, however, would cost a Coulomb energy of about 10 eV for two Cu $3d$ holes on one copper site. On the other hand, less energy is needed to create holes on the oxygen sites. The creation of holes on oxygen sites may start well below $x=6.5$ due to partial ordering of O(1) in chain fragments with more than two chain links.

As a consequence of the strong on-site correlation effects on the copper sites, an upper Hubbard band (UHB) and a lower Hubbard band (LHB) are formed in $YBa_2Cu_3O_6$ instead of a half-filled Cu $3d_{x^2-y^2}$-O $2p_{x,y}$ $\sigma^*$ band as predicted by LDA (Ref. 24) band-structure calculations. An O $2p_{x,y}$ band should appear in between. This corresponds to a model describing the late transition-metal oxides as charge transfer insulators.[25] In this model, with increasing $x$, holes are formed in the valence band (VB), having predominantly O $2p$ character. Exchange interactions between Cu $3d_{x^2-y^2}$ and O $2p_{x,y}$ orbitals, leading to a pairing of the spin of the Cu $3d^9$ hole with that on the neighboring oxygen atoms, form the highest state in the VB, the Zhang-Rice singlet.[26,27]

The $p$-type nature of the electronic structure of $YBa_2Cu_3O_7$ was deduced from chemical arguments, from Hall effect measurements,[28] EELS,[29] and XAS.[30,31] Low-energy excitations studied by EELS (Ref. 32) as well as optical investigations showed a composite plasmon line indicating that holes appear in the $CuO_2$ planes as well as in the $CuO_3$ chain. The orbital character of unoccupied states near $E_F$ was studied by polarization-dependent EELS on single-crystalline $YBa_2Cu_3O_x$ as a function of oxygen concentration, and was in accord with unoccupied Cu $3d_{x^2-y^2}$ and O $2p_{x,y}$ states with $\sigma$ bonding.[33] Similar results were also derived from NMR experiments.[34,35] On the other hand, in many theoretical papers, the importance of unoccupied Cu $3d_{3z^2-r^2}$ and O $2p_z$ states for HTSC cuprates has been emphasized.[36–38] A large contribution to the electronic structure close to the Fermi level ($E_F$) from unoccupied states with Cu $3d_{3z^2-r^2}$ symmetry was derived from polarized XAS investigations of $YBa_2Cu_3O_{6.9}$ single crystals by Bianconi *et al.*[39] However, XAS investigations on other $p$- and $n$-type doped cuprates showed that $3d_{3z^2-r^2}$ states contribute less than 5% to the unoccupied Cu $3d$ states near $E_F$.[40–44]

Optical investigations[45–47] on twin-free domains of $YBa_2Cu_3O_x$ single crystals revealed an appreciably higher frequency for the plasmon edge by light polarized parallel to the chains ($\mathbf{E}\|b$), compared to that for $\mathbf{E}\|a$. This higher plasmon frequency for $\mathbf{E}\|b$ was explained by additional holes on the chains. An analogous result was observed by polarized O $1s$ x-ray-absorption investigations.[48] Recently, a series of single domain crystals of $YBa_2Cu_3O_x$ was prepared and investigated by optical spectroscopy[49] and ultrahigh-resolution dilatometry.[50] In this paper we report on polarization-dependent soft x-ray-absorption experiments using mainly the same set of crystals. The aim of these experiments was the investigation of the hole distribution on all oxygen and copper sites as a function of oxygen content.

## II. EXPERIMENT

$YBa_2Cu_3O_6$ crystals were obtained by annealing as-grown $YBa_2Cu_3O_x$ crystals for 2 days at 700 °C in a vacuum of about $10^{-9}$ mbar. $YBa_2Cu_3O_7$ crystals were prepared by annealing a single crystal in an oxygen atmosphere at 200 bar and at 380 °C for 3 weeks. Single-domain crystals with different oxygen content were

prepared by annealing twinned $YBa_2Cu_3O_7$ crystals at distinct oxygen pressures and subsequent rapid cooling as described by Jorgensen *et al.*[12] The crystals were detwinned by applying an uniaxial pressure to one of the faces parallel to the *c* axis at about 400 °C. The process was controlled by a microscope using polarized light. Details on the crystal growth and preparation of single-domain crystals were described by Erb *et al.*[51] and Zibold *et al.*[52] In our case, the crystals were grown in $ZrO_2$ crucibles stabilized by $Y_2O_3$ and hence were free from Al or Au contaminations. The Zr content measurement by atomic absorption spectroscopy was found to be below the detection limit ( $<0.007$ Zr atoms/unit cell). Well-reflecting (001) surfaces were obtained by cutting off several slices about 100 nm in thickness with an ultramicrotome using a diamond knife. Beside the uppermost layers, these surfaces are stable in air as demonstrated by repeated optical investigations at time intervals of several months, as well as by the absence of a line at 534 eV in the O 1*s* absorption spectrum, which is observed in slightly decomposed cuprates. The size of the crystals was up to 2 mm by 2 mm in the *a*,*b* plane and about 0.3 mm in the *c* axis. Twelve samples were investigated, nine of them exhibiting orthorhombic crystal structure and superconductivity.

One of the major problems in this type of experiment is the determination of the exact number of oxygen atoms per formula unit (i.e., $x$). This can be determined most precisely using neutron diffraction. For these investigations, however, crystals with a volume of at least 1 $mm^3$ are required. Polycrystalline samples[12] and subsequent titration or thermogravimetric analysis have been used to establish a correlation between $x$ and the annealing conditions. In the present study $x$ values (Table I) have been derived using a similar procedure as that described in Ref. 12. The application of this correlation to single-crystalline samples can introduce some errors: the diffusion of oxygen in single crystals is slower than in polycrystalline materials, and the purity of single crystals can be less than that of polycrystalline materials, since for the synthesis of the latter high-purity chemicals are sintered at temperatures below the melting point of $YBa_2Cu_3O_x$. The preparation of single crystals on the other hand needs melting of the materials, and therefore, the contact of the melt with the crucible, especially $Al_2O_3$, or ZnO or Au crucibles, can contaminate the crystal. This may be the reason why lower $T_c$ values are observed for single crystals when compared with those of polycrystalline samples. Another problem is the $BaCuO_2$-CuO flux needed for the growth of single crystals, as sometimes the crystals grow as a stack of platelets with thin layers of flux in between. The $YBa_2Cu_3O_6$ crystals show a strong phonon peak followed by a strong dip at about 80 meV in the optical reflectance spectrum. This is evidence for these samples to be nonmetallic with $x \approx 6.0$.

TABLE I. Comparison of the number of oxygen atoms per formula unit derived from the preparation conditions, $x_p$, and from neutron diffraction, $x_n$. The superconducting transition temperature $T_c$ is given as further parameter.

| $x_p$ | $x_n$ | $T_c$/K |
|---|---|---|
| 7.00±0.02 | 7.00±0.01 | 87.4 |
| 6.95±0.03 | 6.97±0.01 | 91.4 |
| 6.95±0.03 | | 91 |
| 6.75±0.05 | | 81 |
| 6.73±0.05 | | 76 |
| 6.59±0.05 | | 60 |
| 6.57±0.05 | | 55 |
| 6.50±0.05 | 6.49±0.01 | 43 |
| 6.39±0.05 | | 18 |
| 6.15±0.05 | | 0 |
| 6.00±0.03 | | 0 |
| 6.00±0.03 | | 0 |

Three crystals were analyzed by a complete structure analysis using neutron-diffraction techniques. The measurements were performed on the four-circle diffractometer $5C_2$ at the Orphée reactor CE-Saclay. Typically 1200 reflections in a half-sphere were detected leading to 400 independent observations after averaging in the orthorhombic space group $P_{mmm}$. The refinement of the occupancies determined the oxygen concentrations with a precision of about 0.01 atoms per unit cell. No residual O(5) occupancy was observed. Our crystals show an exact 1:2:3 stoichiometry for Y:Ba:Cu and no Cu deficiency as were found in other crystals. Oxygen concentrations of 7.00, 6.97, and 6.49 (see Table I), respectively, were derived for a sample annealed in 200 bars of oxygen, a sample near to the maximum $T_c$, and a sample prepared to have $x=6.5$. The superconducting transition temperatures of the samples, measured by a superconducting quantum interference device (SQUID), are given in Table I.

Polarized O 1*s* and Cu 2*p* absorption edges were recorded using synchrotron radiation from the SX700/II monochromator[53] operated by the Freie Universität Berlin at BESSY. The degree of linear polarization, estimated to be 97±1%,[40] was taken into account for the evaluation of the measured spectra. The intensity variation of the synchrotron radiation beam as a function of energy mainly due to contaminations of the optical components of the monochromator was derived from total-electron-yield measurements of a clean gold surface. The vacuum in the sample chamber was better than $5\times10^{-10}$ mbar during the measurements. Changes in the energy calibration for the monochromatic light were detected by repeated total-electron-yield measurements of the Cu 2*p* absorption line of CuO and the observation of the Ne 1*s* absorption line near 867 eV. Absolute energies were in fair agreement with EELS results for equivalent samples. The relative energy scales for different measurements are correct within better than 0.1 eV. The energy resolution was determined by a study of the Ne 1*s* absorption line at 867 eV using a gas ionization cell.[40] According to the $\Delta E \propto E^{3/2}$ law, valid in the grazing-incidence regime for plane-grating monochromators, the energy resolution $\Delta E = 440$ meV at the Ne 1*s* absorption edge yields an instrumental resolution of $\Delta E = 210$ and 500 meV at the energy of the O 1*s* and Cu 2*p* absorption thresholds, respectively.

The samples were mounted on a manipulator by which they could be rotated around the vertical axis and a hor-

izontal axis. This allowed the orientation of the $a$, $b$, and $c$ axes of the samples to any angle required for measurement with respect to the electrical field vector of the linear polarized synchrotron light. The samples were adjusted with their (001) surfaces perpendicular to the light beam using zero-order light and a mirror on the sample holder. The maximum in the intensity of the O 1$s$ edge at $\approx 528.5$ eV for $\mathbf{E}\|b$ orientation was used to obtain an approximate in-plane orientation of the crystal. For a rotation of the crystal around its $c$ axis by an angle of $\theta$, the total intensity $I(\theta)$ depends on the intensities $I_a$ and $I_b$ for $\mathbf{E}\|a$ and $\mathbf{E}\|b$, respectively, according to $I(\theta)=I_a \sin^2\theta + I_b \cos^2\theta$. The exact orientation $\mathbf{E}\|b(\theta=0)$ was obtained from the intensities measured for three angles with 45° intervals. In order to record $\mathbf{E}\|c$ spectra, the samples were rotated by $\phi=80°$ from normal incidence to nearly grazing incidence. The $\mathbf{E}\|c$ spectra were obtained after correction for a 3% admixture of the in-plane spectrum.

The fluorescence light was detected at an angle of 135° with respect to the photon beam using a Ge detector.[54] The energy resolution of this detector was about 100 eV (FWHM) in the energy range of interest. Different energy windows were set for recording the O 1$s$ and Cu 2$p$ spectra. Thereby contributions from second-order photons from the monochromator and due to the low-energy background were discriminated. In contrast to the total-electron-yield detection technique, the fluorescence-yield mode is characterized by a probing depth of at least 100 nm and hence is not a surface-sensitive detection method.

In order to compare spectra taken for different orientations, the data were recorded up to about 70 eV above the absorption edges, i.e., up to 600 eV and up to 1000 eV for O 1$s$ and Cu 2$p$ absorption spectra, respectively. At about 70 eV above the absorption edges, the final density of states has almost free-electron-like character and hence the spectra may be normalized to tabulated cross sections.[55] From this normalization, the absolute cross sections can be derived in the near-edge region after careful corrections for self-absorption effects using the formalism described in Ref. 56.

We want to point out that the determination of absolute absorption cross sections is not an easy task. The small size of the single crystals investigated required a precise reproducibility of the light spot on the sample independent of the energy setting of the monochromator. The SX700/II monochromator has its exit slit close to the sample, and is therefore well suited for these experiments. The small distance between exit slit and sample, on the other hand, renders an on-line monitoring of the intensity of the incoming monochromatic beam difficult.

The experimental accuracy of the absorption cross section is mainly limited due to necessary corrections for the energy dependence of the polarized photon beam, $I_0$, as derived from a total-electron-yield measurement from a clean gold surface, by a precision of about 3%. Self-absorption corrections are less important for the O 1$s$ spectra and hence introduce errors less than about 3%. In the energy range of the Cu 2$p$ white lines, however, strong corrections have to be considered, which may lead to errors up to about 15%.

## III. RESULTS

### A. O 1$s$ x-ray absorption spectra

To demonstrate the corrections applied to the measured data, the O 1$s$ absorption spectrum of $YBa_2Cu_3O_{6.95}$ recorded for $\mathbf{E}\|b$ is shown in Fig. 2. It is compared with the data corrected for intensity variations of the monochromatic light. The final result including corrections for self-absorption, finite degree of linear polarization of the photon beam, and a small misorientation of the crystal ($<5°$) is given as well.

Figure 3 shows O 1$s$ absorption spectra of $YBa_2Cu_3O_x$ in the range of oxygen concentration $6.0 \le x \le 7.0$ for $\mathbf{E}\|a$, $\mathbf{E}\|b$, and $\mathbf{E}\|c$ polarizations. They were corrected for intensity variations of the monochromatized synchrotron radiation, as well as for self-absorption effects, and they were normalized to the known cross sections in the energy range $580 \le E \le 600$ eV. To ease a comparison of the spectra, they were scaled to the same energy and cross-section ranges. Absorption measurements on pairs of crystals with $x$ values near 6.0, 6.15, 6.58, 6.74 and three crystals with $x$ values of 6.95, 6.97, and 7.00 showed no deviations within the experimental accuracy. They were added, in order to reduce the number of displayed curves and increase the quality of the spectra. Hence, comparisons are restricted to $x$ values of 6.00, 6.15, 6.39, 6.49, 6.58, 6.74, and 6.97.

In general, the present data are in good agreement with XAS spectra presented by Krol *et al.*[48] The relative intensities of the spectra from Ref. 48 for the various polarizations differ slightly from those given in Fig. 3. This can be explained by the fact that in the previous investi-

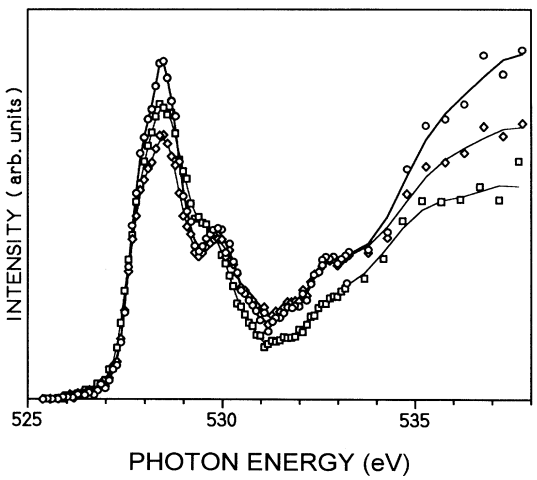


FIG. 2. Demonstration of corrections for the polarized O 1$s$ absorption spectrum ($\mathbf{E}\|b$) for $YBa_2Cu_3O_{6.95}$. Squares, noncorrected data; diamonds, data corrected for the intensity variation of the primary beam $I_0$; and circles, fully corrected data including self-absorption corrections.

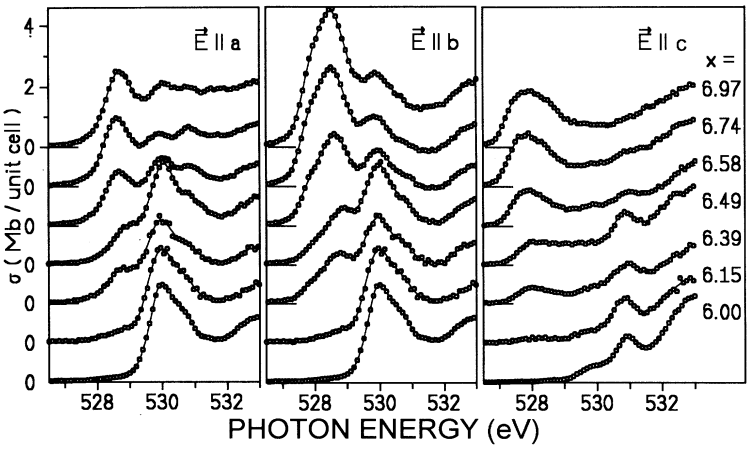


FIG. 3. O 1$s$ absorption spectra of $YBa_2Cu_3O_x$ for $\mathbf{E}\|a$, $\mathbf{E}\|b$, and $\mathbf{E}\|c$.

gation, the spectra have been measured only up to 560 eV, and were normalized to the intensity in the energy range between 540 and 560 eV. However, in the new experiments it was found that in this energy range the density of states (DOS) still shows some polarization dependence and hence this energy range is too low for normalization. Furthermore, in the previous experiment, the $\mathbf{E}\|c$ measurement could not be performed. Instead EELS data were used for which normalization is more difficult.

The spectra for the three polarizations are composed of two main peaks. That at lower energy being strongest for $x=6.97$ decreases for lower $x$ values, while the intensity of the second one shows the opposite oxygen dependence. The onset of the first peak is rather steep for all three polarizations. The slope is comparable with a step edge broadened out by an energy distribution given by the instrumental resolution together with the finite width of the O 1$s$ core level. The energy at half height of the leading edge can, therefore, be assigned to the binding energy (relative to $E_F$) of the 1$s$ core electron of the oxygen atom absorbing the photon. The dependencies of the O 1$s$ threshold energies on oxygen concentration are shown in Fig. 4 for $\mathbf{E}\|a$, $\mathbf{E}\|b$, and $\mathbf{E}\|c$ polarizations. The average O 1$s$ threshold energy is highest for $\mathbf{E}\|a$, lower for $\mathbf{E}\|b$, and lowest for $\mathbf{E}\|c$. For $x=6.0$ there are no longer states at the Fermi level, and hence the binding energy cannot be determined by this method. For $x=6.15$ (insulating state) the crystal was in the tetragonal phase and therefore there is no difference between the spectra for $\mathbf{E}\|a$ and $\mathbf{E}\|b$. It is remarkable, however, that the data points derived in this way for $x=6.15$ are within the trend of the metallic samples. This fact may indicate the existence of localized states at $E_F$ for low doping concentrations. With increasing oxygen concentration from $x=6.39$ to 6.97, the threshold energies decrease by about 0.2, 0.4, and 0.2 eV for $\mathbf{E}\|a$, $\mathbf{E}\|b$, and $\mathbf{E}\|c$, respectively.

The first peak in the spectra (see Fig. 3) is sharpest for $\mathbf{E}\|a$ with a full width at half height of $\Delta E\approx 0.9$ eV. For $\mathbf{E}\|b$, this peak shows a shoulder indicating the composite nature of this feature, and for $\mathbf{E}\|c$, it is significantly broader ($\Delta E\approx 1.4$ eV) as compared to $\mathbf{E}\|a$. All spectra show a strong increase of the intensity in the first peak and a reduction of the second maximum with increasing oxygen concentration. This is similar to the doping dependence of the prepeaks in the O 1$s$ absorption edges of $La_{2-x}Sr_xCuO_4$,[40,57,58] which was interpreted by a doping-induced shift of the Fermi level into the valence band, the creation of holes in the valence band, and a transfer of spectral weight from states in the upper Hubbard band to the upper edge of the valence band.[59–61]

About 3.4 eV above $E_F$, the unoccupied states of hybrids of O 2$p$ states with Ba 5$d$ and Y 4$d$ states are expected.[24] This explains the increase in absorption cross section observed in the corresponding energy range for all measured spectra. As an example the data for $x=6.97$ are shown for all three polarizations in Fig. 5. Above $\approx 533$ eV, the number of data points per eV was reduced, since these measurements were performed mainly for normalization of the spectra in the energy range between 580 and 600 eV. The cross sections in the energy range from 535 to 554 eV differ for the various polarizations (see Fig. 5).

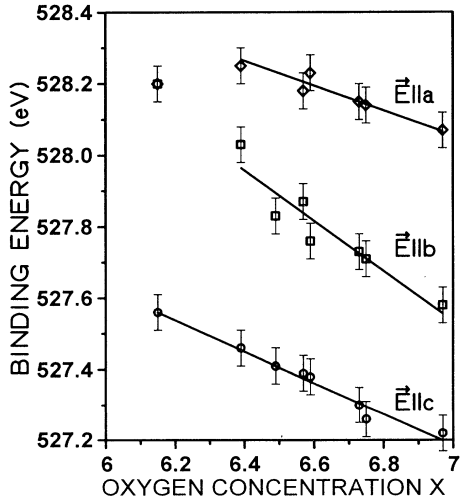


FIG. 4. O 1$s$ threshold energies for $YBa_2Cu_3O_x$ for polarizations $\mathbf{E}\|a$, $\mathbf{E}\|b$, and $\mathbf{E}\|c$. The threshold energies were measured by the energy at half-height of the edge.

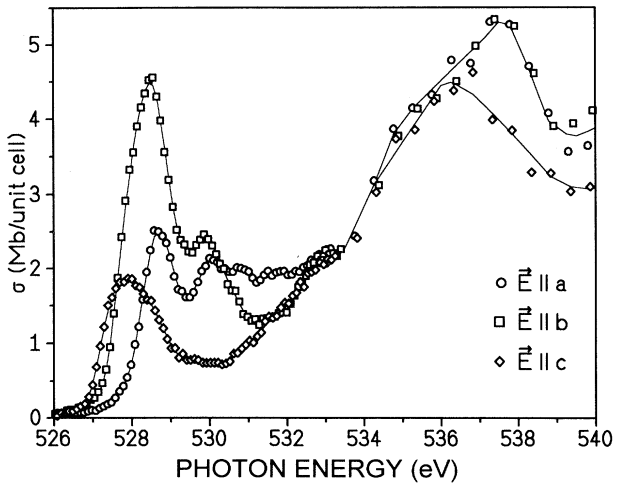


FIG. 5. O 1*s* absorption spectrum of $YBa_2Cu_3O_{6.95}$ for polarizations $\mathbf{E}\|a$, $\mathbf{E}\|b$, and $\mathbf{E}\|c$. Above 533 eV the cross sections are almost independent of $x$.

### B. Cu 2*p* x-ray-absorption spectra

The polarized Cu $2p_{3/2}$ x-ray-absorption spectra for $YBa_2Cu_3O_x$ are shown in Fig. 6 for $\mathbf{E}\|a$, $\mathbf{E}\|b$, and for $\mathbf{E}\|c$. As for other HTSC's, the absorption spectra for $\mathbf{E}\|a$ and for $\mathbf{E}\|b$ show a strong excitonic line near 931 eV due to transitions from the Cu 2*p* core level into unoccupied Cu 3*d* states ($3d^9 \rightarrow \underline{2p}\,3d^{10}$ transitions), which are expected for divalent Cu atoms. Since the intensity of this line is related to the number of unoccupied states involved, our experiment should provide some information on changes in the hole occupancy in Cu 3*d* orbitals with doping.

Upon increasing the oxygen concentration, a shoulder appears on the high-energy side of the main absorption line, which has been ascribed to transitions into ligand

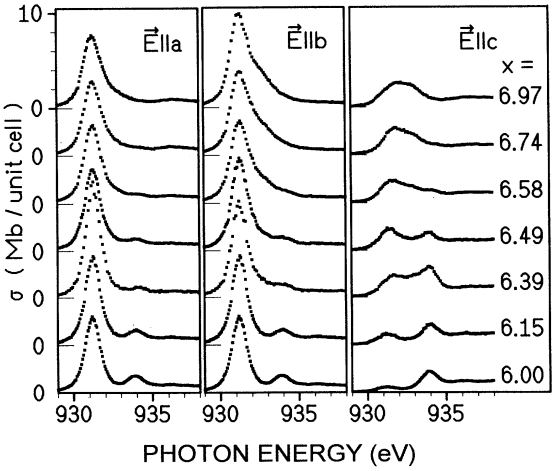


FIG. 6. Cu $2p_{3/2}$ absorption spectra of $YBa_2Cu_3O_x$ for $\mathbf{E}\|a$, $\mathbf{E}\|b$, and $\mathbf{E}\|c$.

hole states[62] ($3d^9\underline{L} \rightarrow \underline{2p}\,3d^{10}\underline{L}$ transitions). This shoulder is much more pronounced for $\mathbf{E}\|b$ than for $\mathbf{E}\|a$. Near 934 eV, another peak is observed in the spectra of samples with low oxygen concentration for all polarizations, but most pronounced for $\mathbf{E}\|c$. As will be shown below, it is due to Cu(1) $3d_{3z^2-y^2}$-O(4) $2p_z$ hybrids of formally monovalent copper. A weak peak is also seen near 936.5 eV mainly for higher oxygen concentration levels and for $\mathbf{E}\|a$ polarization. It is probably related to states in the chain which were also observed in the O 1*s* absorption cross section for $\mathbf{E}\|a$ near 531 eV.

The Cu 2*p* spectra measured for $\mathbf{E}\|c$ do not show such strong white lines as are observed for the in-plane spectra. For high oxygen concentrations they show a broad maximum near 932 eV, that is probably composed of two lines. The intensity of this feature is reduced with the reduction of oxygen content. For low $x$ values, two small lines at the position of the white line and at about 934 eV are observed. For $x = 6.39$ the latter is strongest, which may be due to some contamination of the sample.

## IV. DISCUSSION

### A. Assignment of O 1*s* spectra to oxygen sites

The observed dependencies of the O 1*s* thresholds on oxygen concentration and polarization are a consequence of chemical shifts due to the influence of charges on the oxygen sites, and due to Madelung terms[63,64] determined by the site-specific neighborhood. The experimental threshold energies may be slightly lower than the O 1*s* binding energies in the ground state due to excitonic effects, i.e., the interaction of the core hole with the excited electron. This interaction is small for the oxygen sites in the cuprates since O 1*s* binding energies derived from XPS are close the absorption threshold, and O 1*s* absorption spectra and resonant bremsstrahlen isochromat spectroscopy (BIS) spectra of $Bi_2Sr_2CaCu_2O_8$ show strong similarities.[65] Hence, the O 1*s* binding energies and their dependence on oxygen concentration for the different polarizations allow an assignment of the absorption edges to specific oxygen sites. The O 1*s* binding energies for the different oxygen sites can be estimated using band-structure calculations. However, the relative binding energies for $YBa_2Cu_3O_7$ of such calculations published in different papers[64–68] do not all agree about the sequence in energy. The relative binding energies reported by Krakauer *et al.*[66] are highest for O(2) and decrease relative to O(2) by 0.09, 0.29, and 0.69 eV for O(3), O(1), and O(4), respectively. This result is in fair agreement with the threshold energies shown in Fig. 4. The lowest binding energy is also assigned to O(4) by Zaanen *et al.*[64]

For $\mathbf{E}\|b$, the composite shape of the maximum at 528.5 eV and a much higher cross section is observed for excitation energies up to about 530 eV as compared to $\mathbf{E}\|a$. This observation and the expected similarity of states in the $CuO_2$ plane suggest that the absorption spectrum for $\mathbf{E}\|b$ is composed of a chain [O(1) $2p_y$] and a plane [O(3) $2p_y$] contribution, while that for $\mathbf{E}\|a$ is due to O(2) $2p_x$ states only. These observations imply that the unoccupied oxygen states near the Fermi level are mainly due to

holes in orbitals that are $\sigma$ bonded to copper atoms in agreement with NMR measurements[34,35] and with a calculation of electrical-field gradients[69,4,70] in comparison to NMR results.[69,71] Beside these $\sigma$ bonds, band-structure calculations predict an additional contribution from a narrow O(1) $2p_y$-O(4) $2p_z$-Cu(1) $3d_{y,z}$ band, where the O $2p$ orbitals are $\pi$ bonded to the Cu $3d$ orbitals.[72] A contribution of such hole states was detected by Takigawa *et al.*[35] for the $x=6.95$ case using NMR. The present investigation shows the main contribution of the O(1) absorption for $\mathbf{E}\|b$, but we cannot exclude some spectral weight due to O(4) $2p_y$ ($\pi$-bonding) states for $E\|b$.

The stronger oxygen concentration dependence of the O $1s$ binding energy assigned to O(4) and still stronger dependence for O(1) atoms as compared to O(2,3) atoms can be partially due to increased hole doping in the chains as compared to planes (see below). It may additionally be caused by Madelung shifts due to the structural changes in the chain.

Since there is a small asymmetry of 1.6% between the Cu(2)-O(2) and the Cu(2)-O(3) bond lengths,[73] the symmetry of the Cu(2) $3d_{x^2-y^2}$-O(2,3) $2p_{x,y}$ hybrids in the $CuO_2$ plane may be slightly disturbed. This asymmetry is small, since the major part of the extra cross section observed for $\mathbf{E}\|b$ (see Fig. 5) is at a significantly lower energy, and hence, cannot be due to in-plane oxygen, O(3). In the remainder of this contribution, we shall neglect this asymmetry within the plane and ascribe the observed difference between the $\mathbf{E}\|b$ and $\mathbf{E}\|a$ spectra mainly to contributions from O(1) atoms in the chain.

In the following we will evaluate the site-specific cross sections contributing to the Cu(2) $3d_{x^2-y^2}$-O(2,3) $2p_{x,y}$ hybrids in the $CuO_2$ planes and the Cu(1) $3d_{y^2-z^2}$-O(1,4) $2p_{y,z}$ hybrids in the chains. In a first step, contributions to the spectra from hybrids of O $2p$ with Ba $5d$ and Y $4d$, which dominate the spectra above 532 eV and show almost no dependence on the oxygen concentration, were extrapolated to lower energies and subtracted. Due to the expected symmetry of the O(2,3) $2p_{x,y}$ states in the plane the contribution of O(1) $2p_y$ states should lead to an enhanced cross section for $\mathbf{E}\|b$. But above 530 eV the cross section for $\mathbf{E}\|a$ is larger than for $\mathbf{E}\|b$ (see Fig. 5). This enhanced cross section is found to be correlated with the occupancy of O(1) sites. It is not related to the DOS in the $CuO_2$ plane since the equivalent absorption spectrum for $YBa_2Cu_4O_8$ (Ref. 48) does not show such an enhanced cross section (Fig. 7). For $YBa_2Cu_4O_8$, we observe a dip near 531 eV followed by a maximum at about 533 eV. Unoccupied states related to O $2p$ orbitals hybridized with Ba $5d$ states predicted for this energy region could be the origin for these enhanced cross sections in $YBa_2Cu_3O_7$.[74] They may be shifted to 533 eV in $YBa_2Cu_4O_8$ due to the changed structure of the chains. These Ba $5d$ states are most probably hybridized with O(4) states and are observed mainly in O(4) $2p_x$ orbitals. In the energy range $530 \le E \le 531$ eV, the cross sections for $YBa_2Cu_3O_7$ with $\mathbf{E}\|b$ is almost identical with that for $YBa_2Cu_4O_8$ with $\mathbf{E}\|a$. We conclude, therefore, that there are no ($\le 0.2$ Mb/atom) O(1) states of the chain in this energy range. For $YBa_2Cu_3O_7$, the lower of the cross sections of the $\mathbf{E}\|a$ and $\mathbf{E}\|b$ spectra thus represents the in-plane O(2,3) states, and the extra spectral weight of the $\mathbf{E}\|b$ spectrum below 531 eV is due to O(1) states of the chain.

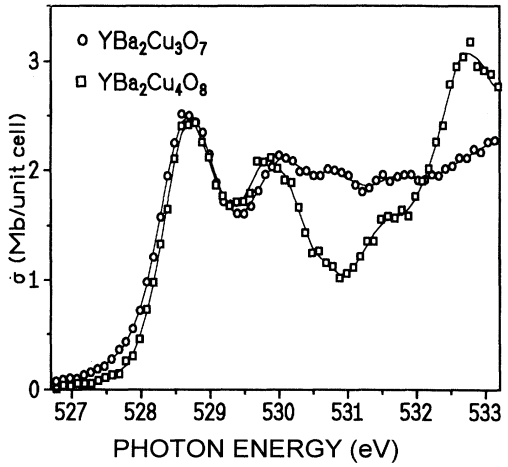


FIG. 7. Comparison of O $1s$ absorption spectra for $\mathbf{E}\|a$ of $YBa_2Cu_3O_7$ and $YBa_2Cu_4O_8$.

The O(2,3) and O(1) spectra for $YBa_2Cu_3O_x$ shown in Fig. 8 were derived from the lower cross sections of the $\mathbf{E}\|a$ and $\mathbf{E}\|b$ spectra and the difference of the $\mathbf{E}\|b$ and $\mathbf{E}\|a$ spectra in the energy range below 531 eV, respectively, after subtraction of the high-energy contributions due to Ba $5d$ and Y $4d$ states. The Ba $5d$ related states near 531 eV change their energy with the oxygen concentration in the chain due to variations in the Madelung energy. Slightly different energies for the Ba $5d$ states were predicted for $x=6$ and 7 by Temmerman *et al.*[24,74] Their band-structure calculations for $YBa_2Cu_3O_6$ showed a maximum for Ba-related states near 2.8 eV above $E_F$, equivalent to about 530 eV for the O(4) $1s$ absorption spectrum. Thus up to 15% of the O(2,3) peak for $x=6$ (Fig. 8) probably is related to Ba states as well.

A comparison of the O(1), O(2,3), and O(4) subspectra of $YBa_2Cu_3O_{6.97}$ with the results of band-structure calculations by Zaanen *et al.*[64] for $YBa_2Cu_3O_7$ is shown in Fig. 9. Here, the threshold energies derived from the measurements are aligned to the Fermi energy of the calculated DOS. The experimental data points for O(2,3) exhibit two maxima representing the holes in the valence band and in the upper Hubbard band. The LDA band-structure calculations, which fail to describe correctly the correlations on the copper sites and therefore cannot predict the upper Hubbard band, show a broad distribution corresponding to a half-filled band. The experimental and calculated spectra for the O(1) site have similar shapes. In the experiment, however, an additional small shoulder is seen at higher energies. Within experimental resolution, the strong rise at the measured onset is compatible with an edge spectrum, while the band-structure-derived DOS shows a significantly lower density at $E_F$. The experimental and calculated spectra for the O(1) and the O(2,3) sites exhibit similar relative weights. The experimental spectral weight for the apical oxygen, in par-

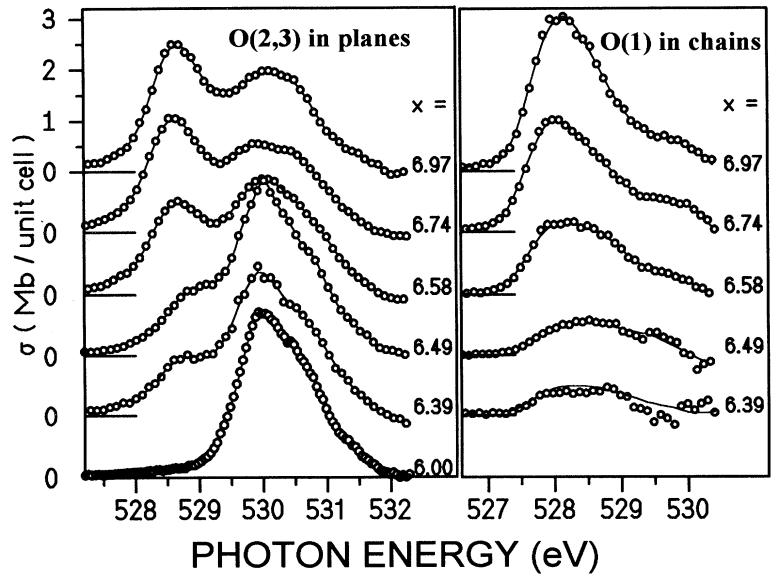


FIG. 8. O 1*s* absorption spectra of O(2,3) in the planes and O(1) in the chains as a function of $x$. The O(2,3) spectra are evaluated from the spectra for $\mathbf{E}\|a$ (Fig. 3) after subtraction of states due to hybridization with Ba or Y (see text). The accuracy of the data is $\approx 5\%$ for energies up to 529 eV and rises to 0.5 Mb/unit cell at higher energies. The O(1) spectra are derived from the enhanced spectral weight for $\mathbf{E}\|b$ relative to that for $\mathbf{E}\|a$.

ticular at 1.5 eV above $E_F$, is considerably reduced in comparison with that derived from the LDA calculation. Self-interaction corrected LDA calculations could describe the UHB in $YBa_2Cu_3O_x$ in a similar way as in $La_2CuO_4$,[3–5] and it would be also interesting to compare with the results of such calculations in the present case.

The dependence of the O 1*s* spectra of the $CuO_2$ planes on oxygen doping shown in Fig. 8 exhibits a clear transfer of spectra weight from the second peak ($E \approx 530$ eV), related to the upper Hubbard band, to the first peak ($E \approx 528.6$ eV), related to the unoccupied part of the valence band, similar to the case of $La_{2-x}Sr_xCuO_4$.[40,57,58] The VB peak with a full width at half maximum of $\Delta E = 0.9$ eV exhibits an increasing cross section starting near the tetragonal-to-orthorhombic phase transition at $x \approx 6.4$ saturating near $x = 7$. The spectral weight related to the UHB (and possibly to some Ba-related states) decreases upon hole doping of the $CuO_2$ plane.

The absorption spectra of the O(1) site (see Fig. 8) show a strong peak at $E \approx 528.2$ eV, with a small shoulder $\approx 1.3$ eV above the main peak. The origin of this shoulder may be due to Ba-related oxygen hybrids or from a small amount of spectral weight related to the UHB of the chains. The shape of the O(1) peak does not change significantly with oxygen concentration $x$. The integral of the valence-band peak of the O(1) atom is about three times larger than that for O(2,3) atoms in the plane. The unchanged shape of the O(1) 1*s* absorption spectrum can be understood by the fact that the number of holes per O(1) atom is nearly constant for different $x$; the increase of the cross section is mainly due to an increasing number of O(1) atoms upon doping.

### B. Number of holes on oxygen sites

A determination of the hole concentration from the O 1*s* absorption spectra is not possible without an under-

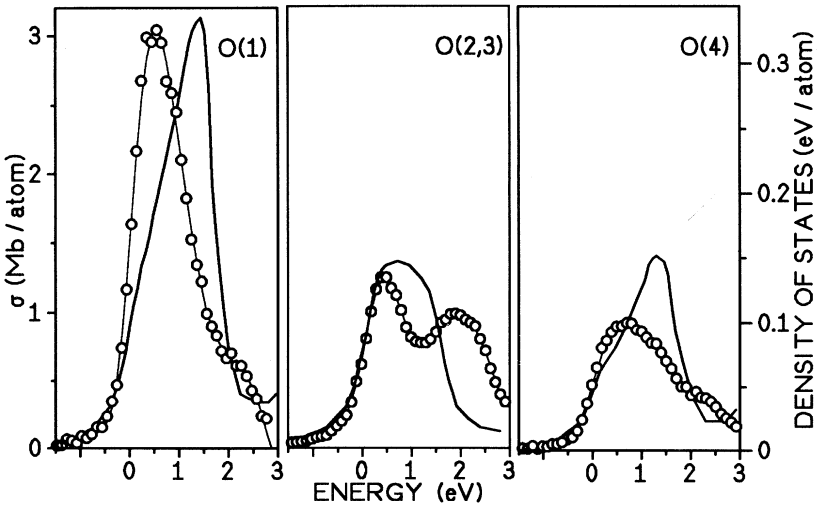


FIG. 9. Comparison of experimental atomic O 1*s* cross sections (symbols) with LDA-band-structure calculated DOS for $YBa_2Cu_3O_7$ as obtained by Zaanen *et al.* (Ref. 64).

standing of the electronic structure and the effects involved in these experiments. Theoretical calculations of electronic structure of cuprates using LSD-SIC,[3-5] the single-band Hubbard model,[75] the $t$-$J$ model,[26] or cluster calculations for the charge-transfer model[60] may be employed for comparison with the experimental data. Up to now, however, there are no such calculations of cross sections for XAS spectra of cuprates. In an ionic model for the undoped compound $YBa_2Cu_3O_6$ Cu(1) and Cu(2) would be in a $3d^{10}$ and $3d^9$ configuration, respectively, and the O atoms would be in a $2p^6$ configuration. Assuming a charge-transfer model without hybridization and a change of the $3d$ count of Cu(1) atoms by 1, in the doped system $YBa_2Cu_3O_7$ the holes would be formed on O sites and the total number of holes on O sites would be 1. However, due to a strong hybridization of Cu $3d$ states with O $2p$ states, O $2p$ states are mixed into the UHB. Doping leads to a spectral weight transfer of states from the UHB to the Fermi level in the valence band.[60] Therefore, the number of hole states observed in the VB peak corresponds probably to slightly less than 1 hole on O sites. On the other hand, the spectral weight transfer of O $2p$ states from the UHB is rather small and therefore, we assume in the following that the integrated cross section of the VB peaks measured for the seven O sites in $YBa_2Cu_3O_7$, i.e., 15 MbeV, is equivalent to one hole. The rather high hole concentration of 0.6 holes in the chain, i.e., 0.34 holes on O(1) and 0.13 holes per O(4), respectively, is responsible for a very low UHB in the O $1s$ absorption spectrum as observed in Fig. 8. In Table II, a comparison of the number of holes resulting from the present investigation and previously published values is given.

The site-specific and oxygen concentration-dependent hole numbers as shown in Fig. 10 were derived from the integrated cross sections of the first absorption peak in the O $1s$ spectra of the O(1) and O(2,3) atoms (Fig. 8), and the O(4) atom ($\mathbf{E}\|c$ spectrum in Fig. 3). They were normalized to one hole for 15 MbeV. The main uncertainty in this evaluation (in the order of 7%) is introduced by the subtraction of the overlap of the second peak in the spectra. The relative amount of transfer of spectral weight from the UHB may differ for the different oxygen sites and thereby influence the relative hole concentrations to some extent. The number of holes does not only depend on the oxygen concentration but also on the length of chainlets. This may be the reason for the scatter in the hole concentration for the different samples.

About 0.2 holes on oxygen sites are observed in one $CuO_2$ plane unit for $YBa_2Cu_3O_7$. This value is slightly higher than in the case of $La_{2-x}Sr_xCuO_4$, with $x=0.15$. The enhanced concentration of holes on the O(1) atoms as compared to the O(4) atoms can be understood keeping in mind that the O(4) atoms are covalently bound only to one Cu(1) and to two O(1) neighbors, while the O(1) atoms are bound to two Cu(1) and four O(4) atoms. This leads to a larger splitting between bonding and antibonding $\sigma$ bands and, therefore, to more holes on O(1) sites.

The hole fractions as given by Krol *et al.*[48] (see Table II) differ slightly from those of the present investigation. This may be explained by the fact that in this previous work the energy for normalization was too low and self-absorption effects were not considered. The hole occupancies may be compared with calculated values,[74,76,77] and with results from NMR investigations combined with calculations of the electrical-field gradient,[69,71] as given in Table II.

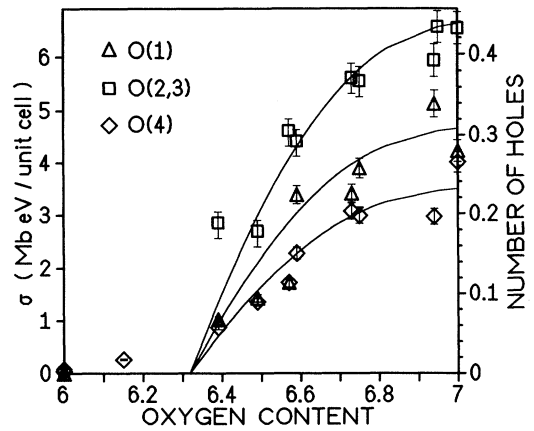


FIG. 10. Hole concentrations on oxygen sites as a function of doping as derived from the absorption cross sections. A total of one hole per unit formula in $YBa_2Cu_3O_7$ was assumed. The lines are guides to the eye. Since the experimental precision of the data points is $\approx 5\%$, the rather big scatter may be understood by different chain lengths in the crystals.

The integrated O $1s$ cross sections for one $CuO_2$ unit in the plane for transitions into the VB and into the second maximum, which are mainly attributed to the UHB, are shown in Fig. 11 as a function of oxygen content. The cross section for excitation into the valence band rises from zero in the case of the undoped ($x=6$) crystal to $\approx(3.1\pm0.2)$ MbeV/(unit cell and plane), saturating near maximum doping ($x=7$). The spectral weight of the UHB, observed in the O $1s$ spectra due to hybridization, decreases upon hole doping of $YBa_2Cu_3O_6$ from $(4.5\pm0.6)$ MbeV (indicated by a horizontal line in Fig. 11) and shows a small upturn close to $x=7$ at $(3\pm0.3)$

TABLE II. Distribution of holes on different oxygen sites in $YBa_2Cu_3O_7$, as obtained in the present experimenst (XAS). For comparison, also the result of previous XAS determinations (XAS1) by Krol *et al.* (Ref. 48), of band-structure calculations (BSC) by Temmerman *et al.* (Ref. 24), of calculations using a three-band model with LDA parameters (3BM) by Oles *et al.* (Ref. 76), of cluster calculations using self-consistent field approximations (SCF) of Mei *et al.* (Ref. 77), and of NMR results combined with calculations of the electric-field gradients (EFG) by Alloul *et al.* (Ref. 34) are presented.

| Site | XAS | XAS1 | BSC | 3BM | SCF | EFG |
|---|---|---|---|---|---|---|
| O(1) | 0.34±0.03 | 0.27 | 0.17 | 0.22 | 0.38 | 0.30 |
| O(2) | 0.10±0.01 | 0.13 | 0.14 | 0.19 | | 0.12 |
| O(3) | 0.10±0.01 | 0.13 | 0.16 | 0.19 | | 0.13 |
| O(4) | 0.13±0.01 | 0.10 | 0.10 | 0.12 | 0.06 | 0.14 |

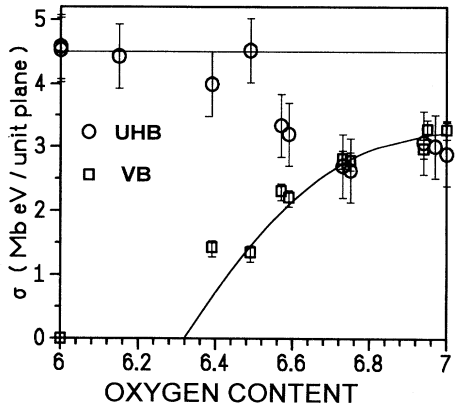


FIG. 11. Integrated cross section of the valence band (squares) and the upper Hubbard band (circles) as a function of doping ($x$) for a single $CuO_2$ plane. A horizontal line indicates the maximum cross section of the UHB.

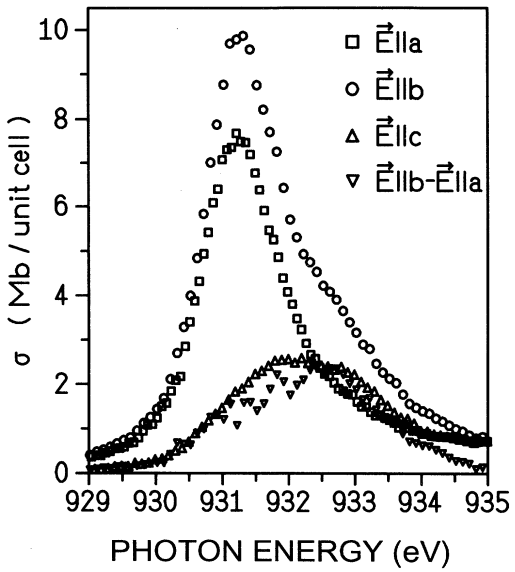


FIG. 12. Cu $2p_{3/2}$ absorption spectrum of $YBa_2Cu_3O_{6.97}$ for polarizations $\mathbf{E}\|a$, $\mathbf{E}\|b$, and $\mathbf{E}\|c$. The difference of the cross sections for $\mathbf{E}\|b$ and $\mathbf{E}\|a$ is nearly equal to the $\mathbf{E}\|c$ spectrum.

MbeV. The spectral weight in the UHB of $YBa_2Cu_3O_6$ is stronger than that of the VB of $YBa_2Cu_3O_7$, and about two times the spectral weight in the UHB of $La_2CuO_4$.[40,57,58] The different spectral weights in the UHB for $YBa_2Cu_3O_6$ and $La_2CuO_4$ may be partially due to different hybridization strengths within the $CuO_2$ planes of these compounds. A stronger contribution arises probably from states near 531 eV in the case of $YBa_2Cu_3O_7$ and near 533 eV in the case of $YBa_2Cu_4O_8$ (see Fig. 7). The different chain structures of $YBa_2Cu_3O_7$ and of $YBa_2Cu_4O_8$ could be the reason for the energy difference of this spectral contribution. Ba $5f$ states hybridized to O(4) atoms may also cause this spectral weight near 530 eV. We observe that these states increase with the amount of O(1) atoms and, therefore, may cause the upturn of the spectral weight in the UHB near $x=7$ (see Fig. 11).

The doping dependence of unoccupied states of the apical oxygen site (see Fig. 3) seems to reflect a similar transfer of spectral weight from the UHB to the VB as in case of plane states. However, the doping level in the chain is much higher than in the plane, and therefore no UHB peak is observed for O(4) similar to O(1). The peak at $\approx 531$ eV is certainly not due to the UHB because it is $\approx 4$ eV above $E_f$, while the UHB in the planes is only $\approx 2$ eV above $E_F$. A comparison with our Cu $2p$ data (see below) provides evidence that the maximum near 531 eV is caused by unoccupied O $2p$ states of the O(4)-Cu(1)-O(4) dumbbell. Therefore, the cross section of this peak is a measure of the number of dumbbells in the system and hence related to the concentration of formally monovalent Cu(1) atoms.

### C. The Cu 2p spectra

For a discussion of the unoccupied states of copper, the Cu $2p$ absorption spectra of $YBa_2Cu_3O_{6.97}$ for $\mathbf{E}\|a$, $\mathbf{E}\|b$, and $\mathbf{E}\|c$ together with the difference of the $\mathbf{E}\|b$ and $\mathbf{E}\|a$ spectra are shown in Fig. 12. As has been pointed out above, the main contribution to the unoccupied states of copper in the $CuO_2$ planes has Cu(2) $3d_{x^2-y^2}$ orbital character, and thus the absorption spectra from Cu(2) atoms should by symmetric with respect to $\mathbf{E}\|a$ and $\mathbf{E}\|b$ polarizations. The $\mathbf{E}\|a$ spectrum, therefore, represents the absorption spectrum of Cu(2) atoms. It shows a narrow peak (the so-called white line) at about 931 eV with a shoulder at the high-energy side. The white line has been assigned to Cu $3d9 \rightarrow$Cu $2\underline{p}3d^{10}$ transitions while the shoulder has been interpreted as a Cu $3d^9\underline{L} \rightarrow$Cu $2\underline{p}3d^{10}\underline{L}$ transition where $\underline{L}$ denotes a hole on the ligand (oxygen) sites. The reason why, contrary to the situation in O $1s$ spectra, transitions into the UHB appear at lower energy than transitions related to hole states on O sites is the strong Coulomb interaction between Cu $3d$ states and the core hole in Cu $2p$ states.[78] Recently, van Veenendaal and Sawatzky[79] have pointed out that due to the strong Coulomb interaction between the core hole and the holes on O sites, the latter may be pushed to neighboring Cu sites. This leads to further contributions to the white line, while the spectral weight of the shoulder is only due to transitions where the holes on O sites remain at the photoexcited Cu atoms.

Since the main contributions to the unoccupied states of copper in the $CuO_3$ chains have Cu(1) $3d_{y^2-z^2}$ orbital character, the absorption spectra for Cu(1) should be symmetric with respect to $\mathbf{E}\|b$ and $\mathbf{E}\|c$ polarizations. The difference spectrum ($\mathbf{E}\|b-\mathbf{E}\|a$), shown in Fig. 12, should therefore represent the absorption due to Cu(1) and should correspond to that measured for $\mathbf{E}\|c$. This is actually the case as can be seen from the comparison between the two spectra. These Cu(1) spectra are significantly broader than those observed for Cu(2) and are probably composed of three absorption lines. The lower-energy contribution at about 931 eV can be as-

signed to Cu(1) $3d^9 \rightarrow$Cu(1) $2\underline{p}3d^{10}$ transition with $(y^2-z^2)$-orbital character and to Cu(2) $3d^9 \rightarrow$Cu(2) $2\underline{p}3d^{10}$ transition with $(3z^2-r^2)$-orbital character. The transition probabilities for excitations into unoccupied states with $3d_{3z^2-r^2}$ symmetry for $\mathbf{E}\|c$ are four times larger than for $\mathbf{E}\|a$ or $\mathbf{E}\|b$, as can be derived from Clebsch-Gordon coefficients. The slightly lower cross section observed for the difference spectrum in Fig. 12, indicates therefore, only a small contribution with $3d_{3z^2-r^2}$ orbital character. The main spectral weight in the Cu(1) spectrum, however, is due to $3d^9\underline{L} \rightarrow 2\underline{p}3d^{10}\underline{L}$ transitions, since nearly all spectral weight of the UHB ($2\underline{p}3d^{10}$ final states) is transferred into the top of the valence band. This situation may be compared to the case of $NaCuO_2$, where the $3d^{10}$ line has disappeared almost completely.[79,80] The Cu(1) $2\underline{p}3d^{10}\underline{L}$ peak of the chain is observed at the same energy as the Cu(2) $2\underline{p}3d^{10}\underline{L}$ maximum of the planes. The origin of a third peak in the $\mathbf{E}\|c$ spectrum observed at $\approx$934 eV for low dopant concentrations will be discussed below.

The integrated Cu $2p_{3/2}$ absorption cross section of the near-edge structure (white line including the shoulder) as a function of $x$ for the two copper sites is shown in Fig. 13. A nearly constant hole density on the Cu(2) sites (deduced from the $\mathbf{E}\|a$ measurements) is observed, while that on the Cu(1) sites (deduced from the $\mathbf{E}\|c$ measurements) is rather small for $YBa_2Cu_3O_{6.0}$. The latter increases upon oxygen doping to about the same value as observed for the Cu(2) sites, due to the formation of a Cu(1) $3d^9\underline{L}$ ground state. The small cross section left for $\mathbf{E}\|c$ and $x=6.0$ may be assigned to the Cu(2) $3d_{3z^2-r^2}$ orbitals in the UHB of the planes.

For a further discussion of the ligand holes observed in the Cu $2p$ absorption spectra, the absorption line at 931 eV (white line) of $YBa_2Cu_3O_{6.0}$ for $\mathbf{E}\|a$ was fitted by a convolution of a Gaussian and a Lorentzian, and subtracted from the spectra for $\mathbf{E}\|a$ for crystals with different oxygen content. The resulting spectra in Fig. 14 (left) show Cu $3d^9\underline{L} \rightarrow$Cu $2\underline{p}3d^{10}\underline{L}$ transitions of Cu(2) in the plane at $\approx$932 eV. These spectra are compared with the result for the Cu(1) atoms in the chain derived as the difference of the full Cu $2p$ absorption spectra for $\mathbf{E}\|b$ and $\mathbf{E}\|a$ (right). The transitions related to ligand holes in the Cu $2p$ absorption spectra, similarly as those in the O $1s$ absorption spectra (see Fig. 8), exhibit significantly higher concentrations in the chain than in the planes. The ratio of the number of ligand holes observed in the Cu(1) and Cu(2) absorption spectra is about $3.3\pm0.4$, in good agreement with the O $1s$ results.

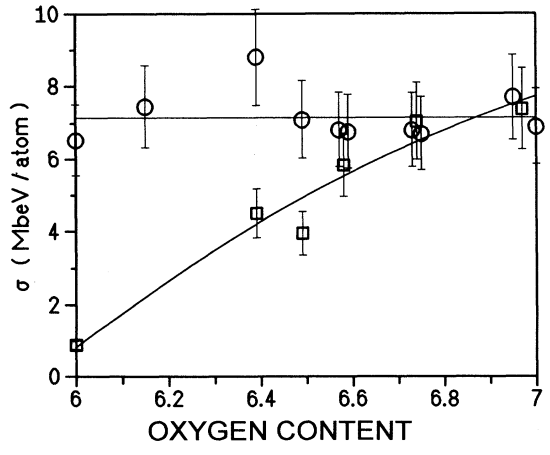


FIG. 13. Doping dependence of Cu $2p_{3/2}$ near-edge absorption cross section for Cu(1) (squares) and for Cu(2) (circles).

The difference spectrum for $\mathbf{E}\|a$ (see Fig. 14, left panel) shows two peaks. The first one at $\approx$932 eV increases upon hole doping, while the intensity of the second one at $\approx$934 eV shows an opposite doping dependence. This second peak is absent in the Cu(1) spectrum (see Fig. 14, right panel) indicating its equal intensity for both the $\mathbf{E}\|a$ and $\mathbf{E}\|b$ polarizations. The third peak in the $\mathbf{E}\|c$ spectrum (see Fig. 6) is observed at the same energy and shows a similar oxygen concentration dependence. From the ratio of the absorption cross sections for the $\mathbf{E}\|c$ and $\mathbf{E}\|a$ (or $\mathbf{E}\|b$) polarizations at $\approx$934 eV, which follows the ratio of the matrix elements, we find that these peaks are due to transitions into the same states with Cu $3d_{3z^2-r^2}$ orbital character. The energy difference to the VB peak and the doping dependence of this maximum resembles that of the peak at 531 eV in the oxygen absorption spectrum for $\mathbf{E}\|c$, as shown in Fig. 3. It is ascribed to monovalent Cu(1) in the O(4)-Cu(1)-O(4) dumbbell, and can be observed in many monovalent copper compounds.[81] This maximum can be explained by Cu(1) $4p$ or $4s$ states, which appear in the Cu $2p$ excitation spectra due to hybridization with Cu(1) $3d_{3z^2-r^2}$ orbitals and apical O(4) $2p_z$ orbitals.[82] The integrated cross section of these peaks decreases linearly with increasing oxygen concentration and vanishes for $x=7.0$. A similar dependence of formally monovalent copper on the oxygen concentration was observed by Tranquada *et al.*[18] The spectrum of the sample with $x=6.39$ does not seem to fit into the doping series as shown in Fig. 6. This may be due to some flux material left on the edge of the crystal, which may also contribute to the spectra. Another explanation is related with disorder in the chain fragments, which may be rather strong for this oxygen concentration near the tetragonal-to-orthorhombic transition.

As mentioned above, the Cu $2p$ absorption spectra for $\mathbf{E}\|c$ (see Fig. 6) contains contributions from mainly Cu(1) and possibly from states in the Cu(2) $3d_{3z^2-r^2}$ orbitals. To obtain the amount of these states in the Cu(2) $3d_{3z^2-r^2}$ orbitals, the contribution of the Cu(1) states of the chain as derived from the difference of spectra for $\mathbf{E}\|b$ and $\mathbf{E}\|a$ was subtracted from those for $\mathbf{E}\|c$. The resulting spectra for $x \geq 6.49$ (not shown here) have a peak at the energy of the white line, the integrated cross section of which is about 0.9 MbeV as compared to 12.7 MbeV for the white line without ligand holes. For $x=6.0$ a direct comparison between the spectra for $E\|c$ and $E\|a$ gives about the same ratio. This contribution, when assigned to Cu(2) $3d_{3z^2-r^2}$ orbitals, would result in an admixture of maximal 10% of states in these orbitals

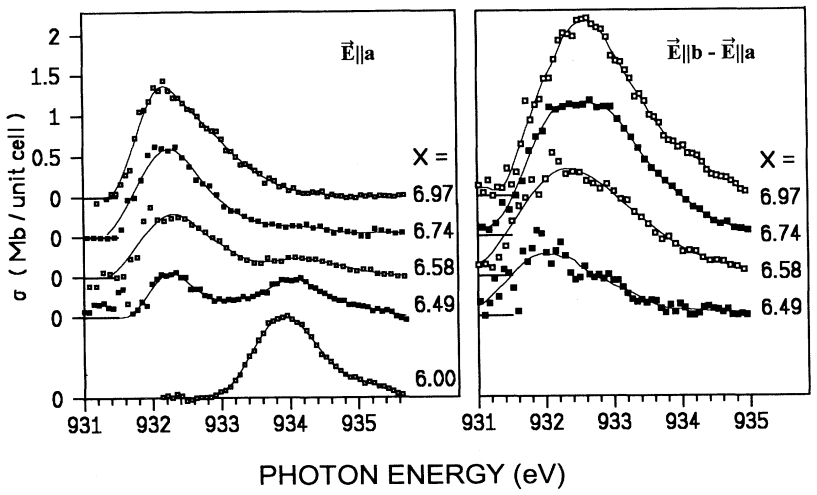


FIG. 14. Cu $2p_{3/2}$ cross section for ligand holes on Cu(2) in the planes ($\mathbf{E}\|a$) of $YBa_2Cu_3O_x$ (after subtraction of the white line), and of Cu(1) in the chains ($\mathbf{E}\|b$-$\mathbf{E}\|a$). The error bars near 931 eV are 1 Mb/unit cell and decrease to 5% and 7% for the plane and the chain spectrum, respectively.

to states with Cu(2) $3d_{x^2-y^2}$ orbital character, in agreement with predictions from band-structure calculations[83] and related investigations for other cuprate superconductors.[40] However, this experiment can only give an upper limit since the measurements performed in grazing incidence are difficult to perform on small crystals, and it cannot be excluded that some CuO is left on the sides of the platelets and contributes to the white lines. The existence of Cu(2) $3d_{3z^2-r^2}$ orbitals may be caused by the slight difference in the Cu(2) and the O(2,3) coordinates in $c$ direction as shown in Fig. 1.

While correlation effects in the $CuO_3$ chain are less important due to the higher doping rate as compared to the $CuO_2$ planes, there is another obvious difference between the planes and the chains, as expressed by the different number of holes on O(1) and O(4) sites. Independent of these differences, the spectral weight in the VB, as observed by O 1$s$ and Cu 2$p$ XAS for the different sites, show almost the same doping dependence as demonstrated in Fig. 15. The $T_c$ dependence of the investigated samples (see Table I) is shown in Fig. 15 as well. Clearly, a strong correlation between the hole concentration and $T_c$ is observed. The $T_c$ dependence differs from the steplike behavior with plateaux near 60 and 90 K that are usually observed for polycrystalline samples.[12] This is probably due to a different degree of order in the single crystals investigated as a consequence of different annealing conditions or storage time at room temperature. The hole concentration and $T_c$ show a threshold near the tetragonal-to-orthorhombic phase transition at $x \approx 6.3$. At lower doping, apparently the two holes introduced per O(1) atom are mainly transferred to the neighboring Cu(1) atoms, which thereby obtain a $3d^9$ configuration, and only a small fraction of holes is transferred to the oxygen sites. The almost linear relation between hole concentration and $T_c$ is in disagreement with the observation of Zhang and Sato,[84] who provide evidence for a trapezoidal shape of the $T_c$ dependence on hole concentration. According to their paper, $T_c$ should be at its maximum value above a concentration of 0.12 holes per $CuO_2$ plane. This behavior and the strong dependence of superconductivity on the order in the chains can be due to local formation of chains, which are necessary for hole doping the $CuO_2$ planes.

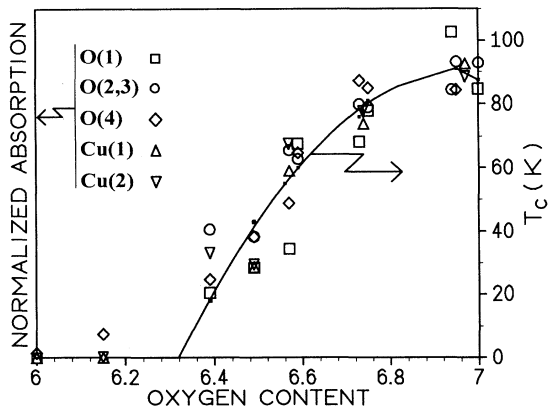


FIG. 15. Doping dependence of valence-band holes measured on oxygen and on copper sites as compared to superconducting transition temperature $T_c$ (dots). The line is a guide to the eye.

## V. CONCLUSIONS

In summary, the distribution of holes on the different oxygen and copper sites have been derived for $YBa_2Cu_3O_x$ in the doping range $6.0 \leq x \leq 7.0$. For low doping concentrations, the holes are located mainly at Cu(1) sites. In the intermediate and high-doping range, fourfold coordinated Cu(1) is dominantly formed and an increasing number of the doped holes is transferred to oxygen atoms. At maximum doping ($YBa_2Cu_3O_7$), about 0.6 holes per $CuO_3$ unit of the chain, or a total charge of nearly one hole is distributed on the four oxygen neighbors of Cu(1). This high level of hole doping in the chain is the origin of its more normal metallic character, as evident from the absence of the UHB in the absorption spectra of the chains.

The charge transferred to the $CuO_2$ planes is much lower than that introduced into the chain upon doping. The band filling in the planes remains close to a half-filling for all doping concentrations. Therefore, on-site correlations play an important role for the electronic structure of the planes. For the highest doping level, a saturation of holes in the planes with 0.2 holes per $CuO_2$ is observed. In the planes, the main electronic states at $E_F$ are in Cu $3d_{x^2-y^2}$-O $2p_{x,y}$ orbitals, while the states with Cu $3d_{3z^2-r^2}$ character contribute less than 10%.

At about 2 eV above $E_F$, spectra weight was observed in O 1$s$ spectra for polarization $\mathbf{E}\|a$, which increases with oxygen concentration, and probably is equivalent to that observed at $\approx 4$ above $E_F$ in $YBa_2Cu_4O_8$. It is tentatively assigned to Ba $5f$ states hybridized to O(1) atoms in the chain.


## ACKNOWLEDGMENTS

We thank M. Domke for his help in running the SX700/II beamline. The high-pressure doped crystal was lent for our experiments by H. Wühl. The help by G. Bräuchle to prepare the $YBa_2Cu_3O_{6.5}$ doped crystal is very much appreciated. We thank K. Urban and T. Woisczyk for $T_c$ measurements. Theoretical support was given by H. Eskes, W. M. Temmerman, and H. Winter. Fruitful discussions with the former as well as with H. Claus and H. Romberg contributed to the interpretation of the data. M. S. Golden's critical reading of the manuscript is very much appreciated. We thank the European Union for support under Contract SC1 CT91-0751. The work at the Freie Universität Berlin was supported by the Bundesminister für Forschung und Technologie, Project No. 05-5KEAXI-3/TP01+TP03.



[1] J. G. Bednorz and K. A. Müller, Z. Phys. B **64**, 189 (1986).
[2] L. F. Mattheiss, Phys. Rev. Lett. **58**, 1028 (1987).
[3] A. Svane and O. Gunnarsson, Europhys. Lett. **7**, 171 (1987).
[4] A. Svane, Phys. Rev. Lett. **68**, 1900 (1992).
[5] W. M. Temmerman, Z. Szotek, and H. Winter, Phys. Rev. B **47**, 11 533 (1993).
[6] H. Verweij, Solid State Commun. **67**, 109 (1988).
[7] J. D. Jorgensen, S. Pei, P. Lightfoot, H. Shi, A. P. Paulikas, and B. W. Veal, Physica C **167**, 571 (1990).
[8] D. J. Werder, C. H. Chen, R. J. Cava, and B. Batlogg, Phys. Rev. B **38**, 5130 (1988).
[9] R. Sonntag, D. Hohlwein, T. Brückel, and G. Collin, Phys. Rev. Lett. **66**, 1497 (1991).
[10] A. A. Aligia and J. Garcés, Physica C **194**, 223 (1992).
[11] G. Uimin and J. Rossat-Mignod, Physica C **199**, 251 (1992).
[12] J. D. Jorgensen, B. W. Veal, A. P. Paulikas, L. J. Nowicki, G. W. Crabtree, H. Claus, and W. K. Kwok, Phys. Rev. B **41**, 1863 (1990).
[13] E. Janod, A. Junod, T. Graf, K.-Q. Wang, G. Triscone, and J. Muller, Physica C **216**, 129 (1993).
[14] R. J. Cava, B. Batlogg, C. H. Chen, E. A. Rietman, C. M. Zahurak, and D. Werder, Nature **329**, 423 (1987).
[15] S. Lapinskas, A. Rosengren, and E. E. Tornau, Physica C **199**, 91 (1992).
[16] P. Steiner, V. Kinsinger, I. Sander, B. Siegwart, S. Hüfner, C. Politis, R. Hoppe, and H. P. Müller, Z. Phys. B **67**, 497 (1987).
[17] H. Guyot, Physica C **180**, 108 (1991).
[18] J. M. Tranquada, S. M. Heald, A. R. Modenbaugh, and Y. Xu, Phys. Rev. B **38**, 8893 (1988).
[19] J. Guo, D. E. Ellis, E. E. Alp, and G. L. Goodman, Phys. Rev. B **42**, 251 (1990).
[20] M. Horvatić, P. Ségransan, C. Berthier, Y. Berthier, P. Butaud, J. Y. Henry, M. Coauch, and J. P. Chaminade, Phys. Rev. B **39**, 7332 (1989).
[21] W. W. Warren, Jr., R. E. Walstedt, G. F. Brennert, R. J. Cava, B. Batlogg, and L. W. Rupp, Phys. Rev. B **39**, 831 (1989).
[22] J. Kircher, M. K. Kelly, S. Rashkeev, M. Alouani, D. Fuchs, and M. Cardona, Phys. Rev. B **44**, 217 (1991).
[23] H. Romberg, N. Nücker, J. Fink, T. Wolf, X. X. Xi, B. Koch, H. P. Geserich, M. Dürrler, W. Assmus, and B. Gegenheimer, Z. Phys. B **78**, 367 (1990).
[24] W. M. Temmerman, Z. Szotec, and G. Y. Guo, J. Phys. C **21**, L867 (1988).
[25] J. Zaanen, G. A. Sawatzky, and J. W. Allen, Phys. Rev. Lett. **55**, 418 (1985).
[26] F. C. Zhang and T. M. Rice, Phys. Rev. B **37**, 3759 (1988).
[27] H. Eskes and G. A. Sawatzky, Phys. Rev. Lett. **61**, 1415 (1988).
[28] N. P. Ong, Z. Z. Wang, J. Clayhold, J. M. Tarascon, L. H. Greene, and W. R. McKinnon, Phys. Rev. B **35**, 8807 (1987).
[29] N. Nücker, J. Fink, J. C. Fuggle, P. J. Durham, and W. M. Temmerman, Phys. Rev. B **37**, 5158 (1988).
[30] J. A. Yarmoff, D. R. Clarke, W. Drube, U. O. Karlsson, A. Teleb-Ibrahimi, and F. J. Himpsel, Phys. Rev. B **36**, 3967 (1987).
[31] P. Kuiper, G. Kruizinga, J. Ghijsen, M. Grioni, P. J. W. Weijs, F. M. F. de Groot, G. A. Sawatzky, H. Verweij, L. F. Feiner, and H. Petersen, Phys. Rev. B **38**, 6483 (1988).
[32] J. Fink, N. Nücker, H. Romberg, and S. Nakai, *High-$T_c$ Superconductors,* edited by A. Bianconi and A. Marcelli (Pergamon, NY, 1989), p. 293.
[33] N. Nücker, H. Romberg, X. X. Xi, J. Fink, B. Gegenheimer, and Z. X. Zhao, Phys. Rev. B **39**, 6619 (1989).
[34] H. Alloul, T. Ohno, and P. Mendels, Phys. Rev. Lett. **63**, 1700 (1989).
[35] M. Takigawa, P. C. Hammel, R. H. Heffner, Z. Fisk, J. L. Smith, and R. B. Schwarz, Phys. Rev. B **39**, 300 (1989).
[36] W. Weber, Z. Phys. B **70**, 323 (1988).
[37] H. Kamimura and M. Eto, J. Phys. Soc. Jpn. **59**, 3053 (1990).
[38] V. I. Anisimov, M. A. Korotin, J. Zaanen, and O. K. Andersen, Phys. Rev. Lett. **68**, 345 (1992).
[39] A. Bianconi, M. De Santis, A. M. Flank, A. Fontaine, P. Lagarde, A. Marcelli, H. Katayama-Yoshida, and A. Kotani, Physica C **153-155**, 1760 (1988).
[40] E. Pellegrin, N. Nücker, J. Fink, S. L. Molodtsov, A. Gutiérrez, E. Navas, O. Strebel, Z. Hu, M. Domke, G. Kaindl, S. Uchida, Y. Nakamura, J. Markl, M. Klauda, G. Saemann-Ischenko, A. Krol, J. L. Peng, Z. Y. Li, and R. L. Greene, Phys. Rev. B **47**, 3354 (1993).
[41] F. J. Himpsel, G. V. Chandrashekhar, A. B. McLean, and M. W. Schafer, Phys. Rev. B **38**, 11 946 (1988).
[42] P. Kuiper, M. Grioni, G. A. Sawatzky, D. B. Mitzi, A. Kapitulnik, A. Santaniello, P. de Padova, and P. Thiry, Physica C **157**, 260 (1989).

[43]M. Abbate, M. Sacchi, J. J. Wnuk, L. W. M. Schreurs, Y. S. Wang, R. Lof, and J. C. Fuggle, Phys. Rev. B **42**, 7914 (1990).
[44]S. Suzuki, T. Takahashi, T. Kusunoki, T. Morikawa, S. Sato, H. Katayama-Yoshida, A. Yamanaka, F. Minami, and S. Takekawa, Phys. Rev. B **44**, 5381 (1991).
[45]M. P. Petrov, A. I. Gratchev, M. V. Krasin'kova, A. A. Nechitailov, V. V. Prokofiev, V. V. Poborchy, S. I. Shagin, and N. F. Kartenko, Solid State Commun. **67**, 1197 (1988).
[46]J. Tanaka, K. Kamiya, and S. Tsurumi, Physica C **153-155**, 653 (1988).
[47]B. Koch, H. P. Geserich, and Th. Wolf, Solid State Commun. **71**, 495 (1989).
[48]A. Krol, Z. H. Ming, Y. H. Kao, N. Nücker, G. Roth, J. Fink, G. C. Smith, K. T. Park, J. Yu, A. J. Freeman, A. Erb, G. Müller-Vogt, J. Karpinski, E. Kaldis, and K. Schönmann, Phys. Rev. B **45**, 2581 (1992).
[49]A. Zibold, K. Widder, H. P. Geserich, G. Bräuchle, H. Claus, H. v. Löhneysen, N. Nücker, A. Erb, and G. Müller-Vogt, Physica C **212**, 365 (1993).
[50]O. Kraut, C. Meingast, G. Bräuchle, H. Claus, A. Erb, G. Müller-Vogt, and H. Wühl, Physica C **205**, 139 (1993).
[51]A. Erb, T. Traulsen, and G. Müller-Vogt, J. Cryst. Growth **137**, 487 (1994).
[52]A. Zibold, M. Dürrler, H. P. Geserich, A. Erb, and G. Müller-Vogt, Physica C **171**, 151 (1990).
[53]M. Domke, T. Mandel, A. Puschmann, C. Xue, D. A. Shirley, G. Kaindl, H. Petersen, and P. Kuske, Rev. Sci. Instrum. **63**, 80 (1992).
[54]The fluorescence detector used was left for our disposal by BESSY.
[55]J. J. Yeh and I. Lindau, At. Data Nucl. Data Tables **32**, 1 (1985).
[56]L. Tröger, D. Arvanitis, K. Baberschke, H. Michaelis, U. Grimm, and E. Zschech, Phys. Rev. B **46**, 3283 (1992).
[57]H. Romberg, M. Alexander, N. Nücker, P. Adelmann, and J. Fink, Phys. Rev. B **42**, 8768 (1990).
[58]C. T. Chen, F. Sette, Y. Ma, M. S. Hybertsen, E. B. Stechel, W. M. C. Foulkes, M. Schlüter, S.-W. Cheong, A. S. Cooper, L. W. Rupp, Jr., B. Batlogg, Y. L. Soo, Z. H. Ming, A. Krol, and Y. H. Kao, Phys. Rev. Lett. **66**, 104 (1991).
[59]M. S. Hybertsen, E. B. Stechel, W. M. C. Foulkes, and M. Schlüter, Phys. Rev. B **45**, 10 032 (1992).
[60]H. Eskes, M. B. J. Meinders, and G. A. Sawatzky, Phys. Rev. Lett. **67**, 1035 (1991).
[61]M. B. J. Meinders, H. Eskes, and G. A. Sawatzky, Phys. Rev. B **48**, 3916 (1993).
[62]A. Bianconi, A. Congiu Castellano, M. De Santis, P. Rudolf, P. Lagarde, A. M. Flank, and A. Marcelli, Solid State Commun. **63**, 1009 (1987).
[63]K. Siegbahn, C. Nordling, G. Johannson, J. Hedman, P. F. Heden, K. Hamrin, U. Gelius, T. Bergmark, L. O. Werme, R. Manne, and Y. Baer, *ESCA Applied to Free Molecules* (North-Holland, Amsterdam, 1969), p. 104.
[64]J. Zaanen, M. Alouani, and O. Jepsen, Phys. Rev. B **40**, 837 (1989).
[65]W. Drube, F. J. Himpsel, G. V. Chandrashekhar, and M. W. Shafer, Phys. Rev. B **39**, 7328 (1989).
[66]H. Krakauer, W. E. Pickett, and R. E. Cohen, J. Supercond. **1**, 111 (1988).
[67]W. E. Pickett, Rev. Mod. Phys. **61**, 433 (1989).
[68]J. Yu, K. T. Park, and A. J. Freeman, Physica C **172**, 467 (1991).
[69]D. J. Sing, K. Schwarz, and P. Blaha, Phys. Rev. B **46**, 5849 (1992).
[70]V. I. Anisimov, J. Zaanen, and O. K. Andersen, Phys. Rev. B **44**, 943 (1991).
[71]F. J. Adrian, Physica C **171**, 505 (1990).
[72]S. Massidda, J. Yu, A. J. Freeman, and D. D. Koelling, Phys. Lett. A **122**, 198 (1987).
[73]M. A. Beno, L. Soderholm, D. W. Capone II, D. G. Hinks, J. D. Jorgensen, J. D. Grace, I. K. Schuller, C. U. Segre, and K. Zhang, Appl. Phys. Lett. **51**, 57 (1987).
[74]W. M. Temmerman, Z. Szotec, P. J. Durham, G. M. Stocks, and P. A. Sterne, J. Phys. F **17**, L319 (1987).
[75]P. W. Anderson, Science **235**, 1196 (1987).
[76]A. M. Olés and W. Grzelka, Phys. Rev. B **44**, 9531 (1991).
[77]C.-J. Mei and G. Stollhoff, Phys. Rev. B **43**, 3065 (1991).
[78]M. Pompa, C. Li, A. Bianconi, A. C. Castellano, S. Della Longa, A. M. Flank, P. Lagarde, and D. Udron, Physica C **184**, 51 (1991).
[79]M. A. van Veenendaal and G. A. Sawatzky, Phys. Rev. B **49**, 3473 (1994).
[80]D. D. Sarma, O. Strebel, C. T. Simmons, U. Neukirch, G. Kaindl, R. Hoppe, and H. P. Müller, Phys. Rev. B **37**, 9784 (1988).
[81]M. Grioni, J. B. Goedkoop, R. Schoorl, F. M. F. de Groot, J. C. Fuggle, F. Schäfers, E. E. Koch, G. Rossi, J.-M. Esteva, and R. C. Karnatak, Phys. Rev. B **39**, 1541 (1989).
[82]P. Marksteiner, P. Blaha, and K. Schwarz, Z. Phys. B **64**, 119 (1986).
[83]J. B. Grant and A. K. Mc.Mahan, Phys. Rev. B **46**, 8440 (1992).
[84]H. Zhang and H. Sato, Phys. Rev. Lett. **70**, 1697 (1993).